URSI GASS 2021, Rome, Italy, 28 August - 4 September 2021

Numerical Study of the Absorbed Power Density Reconstruction for Human Exposure Assessment in Quasi-Millimeter and Millimeter Wave Bands

Shuntaro Omi(1), Ryo Matsumoto(1)(2), Kensuke Sasaki(1), Kanako Wake(1), Ryosuke Suga(2), and Osamu Hashimoto(2)
(1) National Institute of Information and Communications Technology, Tokyo, Japan
(2) Department of Electrical and Electronic Engineering, Aoyama Gakuin University, Kanagawa, Japan

Abstract

A method of evaluating the absorbed power density (APD) is studied to reconstruct the APD from fields measured outside the human body (phantom). It is based on the surface equivalence theorem and the Poggio–Miller–Chang–Harrington–Wu–Tsai (PMCHWT) formulation. The method is numerically studied and the issue related to the separation distance between the device under test (DUT) and the phantom is discussed. An accuracy improvement technique involving the suitable initialization of the iterative matrix solver is also presented.

1 Introduction

Frequencies above 6 GHz are used in communication systems such as the 5th generation communication system (5G) or WiGig. The latest guidelines by ICNIRP and IEEE [1, 2] introduce the absorbed power density (APD) (termed as the epithelial power density in [2]) on the surface of the human body (phantom) as the measure of the local exposure from the device under test (DUT). In the guideline [1], the APD is defined as a basic restriction (dosimetric reference limit (DRL) in [2]) ,i.e., the basic measure of exposure. The incident power density (IPD) in free space is also introduced as a reference level (exposure reference level (ERL) in [2]) that has correlation with the APD and is easier to be measured. However, the necessity of using the basic restriction in reactive near-field regions has been pointed out [1].

In contrast to the IPD for which the measurement method is developed in the several works [3–5], the measurement method for the APD evaluation have not been reported to best of our knowledge. In this work, we propose a novel method which reconstruct the APD from the measurement outside the phantom. By means of the reconstruction, the direct measurement at the phantom's surface is not required which is difficult to be performed. The reconstruction method is based on the one proposed for the noninvasive specific absorption rate (SAR) measurement [6, 7]. The method is based on the surface equivalence theorem and the Poggio–Miller–Chang–Harrington–Wu–Tsai (PMCHWT) formulation [8], and reconstruct the equivalent electromagnetic current on the phantom's surface by solving an integral relation. The method is numerical studied

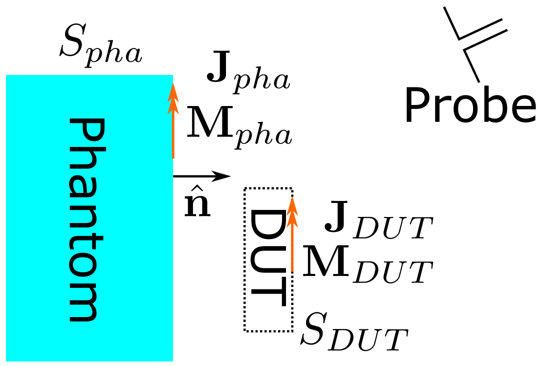

Figure 1. Method of evaluating the APD.

and the accuracy degradation issue is discussed in relation to the separation distance between the DUT and the phantom.

2 Method

The method employed for evaluating the APD is reviewed in this section. The APD is obtained from the electric and magnetic fields on a human body (phantom) as,

$$\mathrm{APD} = -\frac{1}{2}\Re\left[\mathbf{E}\times\mathbf{H}^*\right]\cdot\hat{\mathbf{n}} = \frac{1}{2}\Re\left[\mathbf{M}_{pha}\times\mathbf{J}^*_{pha}\right]\cdot\hat{\mathbf{n}} \quad (1)$$

where $\mathbf{J}_{pha}$ and $\mathbf{M}_{pha}$ are the equivalent electric and magnetic currents (see Fig. 1) on the surface of the phantom (S_{pha}), respectively. These currents are related to the electromagnetic fields on the surface as

$$\mathbf{J}_{pha} = \hat{\mathbf{n}}\times\mathbf{H},\ \mathbf{M}_{pha} = \mathbf{E}\times\hat{\mathbf{n}}. \quad (2)$$

The exposure is assessed by the spatially averaged APD (sAPD) as

$$\mathrm{sAPD} = \frac{1}{A}\iint_A \mathrm{APD}\, da. \quad (3)$$

The averaging area A is 4 cm^2 for frequencies from 6 GHz to 30 GHz [1].

As in Fig. 1, the field is measured outside the phantom by a probe. By means of the surface equivalence, the electric field at the probe position is represented by the equivalent

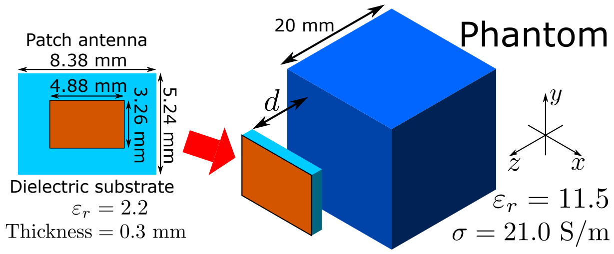

Figure 2. Geometry of numerical results. The design of the patch antennas is also shown.

electromagnetic currents on the surface enclosing the DUT (S_{DUT}) and on the surface of the phantom:

$$\mathbf{E}(\mathbf{r}) = \mathscr{L}^{k_0}(\mathbf{J}_{DUT};\mathbf{r}) + \mathscr{K}^{k_0}(\mathbf{M}_{DUT};\mathbf{r}) + \mathscr{L}^{k_0}(\mathbf{J}_{pha};\mathbf{r}) + \mathscr{K}^{k_0}(\mathbf{M}_{pha};\mathbf{r}), \quad (4)$$

where $\mathbf{J}_{DUT}$ and $\mathbf{M}_{DUT}$ are the equivalent electric and magnetic currents on S_{DUT}, respectively. The integral operators $\mathscr{L}$ and $\mathscr{K}$ use dyadic Green's functions as follows:

$$\{\mathscr{L}/\mathscr{K}\}^k(\mathbf{X};\mathbf{r}) = \iint_S \overline{\mathbf{G}}^k_{EJ/EM}(\mathbf{r},\mathbf{r}')\cdot\mathbf{X}(\mathbf{r}')\,d\mathbf{r}'^2, \quad (5)$$

where $\mathbf{X}$ is the electric or magnetic current and the dyadic Green's functions $\overline{\mathbf{G}}^k_{EJ/EM}$ are for the electric and magnetic currents [9] at the wavenumber of k. S is the surface on which the current is defined, e.g., S_{pha} for $\mathbf{J}_{pha}$. Using the PMCHWT formulation, the currents on S_{pha} are related to those on S_{DUT} as [6,7]

$$\begin{bmatrix}\mathbf{J}_{pha}\\ \mathbf{M}_{pha}\end{bmatrix} = \left(\hat{\mathbf{n}}\times\begin{bmatrix}\mathscr{L}^{k_0}_{PP}+\mathscr{L}^{k_p}_{PP} & \mathscr{K}^{k_0}_{PP}+\mathscr{K}^{k_p}_{PP}\\ -\eta_0\mathscr{K}^{k_0}_{PP}-\eta_p\mathscr{K}^{k_p}_{PP} & \frac{1}{\eta_0}\mathscr{L}^{k_0}_{PP}+\frac{1}{\eta_p}\mathscr{L}^{k_p}_{PP}\end{bmatrix}\right)^{-1} \left(\hat{\mathbf{n}}\times\begin{bmatrix}\mathscr{L}^{k_0}_{PD} & \mathscr{K}^{k_0}_{PD}\\ -\eta_0\mathscr{K}^{k_0}_{PD} & \frac{1}{\eta_0}\mathscr{L}^{k_0}_{PD}\end{bmatrix}\right)\begin{bmatrix}\mathbf{J}_{DUT}\\ \mathbf{M}_{DUT}\end{bmatrix}, \quad (6)$$

where η_0 and η_p are the characteristic impedances of the free space and phantom's medium, respectively. Substituting (6) into (4) leads to an integral equation relating the electric field to the equivalent currents $\mathbf{J}_{DUT}$ and $\mathbf{M}_{DUT}$. The relation is reduced to a matrix equation by discretization with the Rao–Wilton–Glisson (RWG) basis and testing functions [10] and solved in the least squares sense. In this work, we employ an iterative method called LSQR [11] for solving the matrix equation with tolerance ATOL $= 10^{-3}$. Given the equivalent currents $\mathbf{J}_{DUT}$ and $\mathbf{M}_{DUT}$, the electromagnetic currents $\mathbf{J}_{pha}$ and $\mathbf{M}_{pha}$ are obtained using the relation in (6). Finally, the sAPD in (3) is evaluated using the APD given as (1).

3 Numerical Results

The numerical results obtained by electromagnetic field simulations are presented in this section. In the simulation, a patch antenna (DUT) operated at 28 GHz as in Fig. 2 illuminates a phantom of a dielectric cube whose relative permittivity and conductivity are 11.5 and 21.0 S/m, respectively. The separation distance between the phantom and the antenna is d. The electromagnetic fields are simulated by FEKO software [12]. To reconstruct the APD, the electric field is sampled on a sphere with a radius of 50 mm at 6° intervals in the θ and ϕ directions. The APD is reconstructed from the sampled field by the reconstruction method introduced in the previous section.

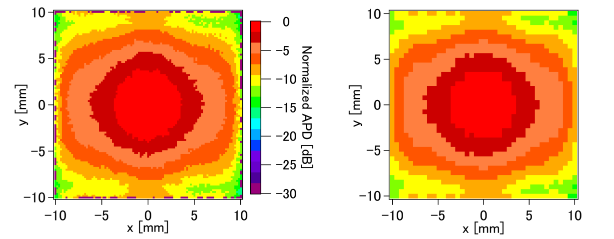

(a) **(b)**

Figure 3. Distributions of the normalized APD for $d =$ 10 mm. (a) Reconstructed result. (b) Reference directly given by the simulation.

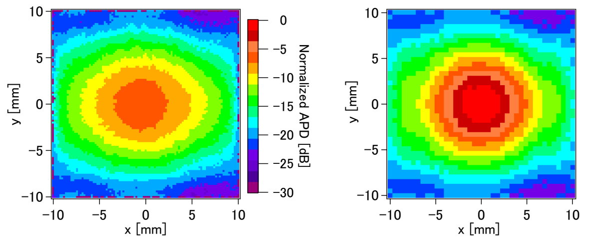

(a) **(b)**

Figure 4. Distributions of the normalized APD for $d =$ 4 mm. (a) Reconstructed result. (b) Reference directly given by the simulation.

Figure 3 shows the APD distribution on S_{pha}. The reconstructed distribution on a phantom's surface facing the antenna (Fig. 3a) is shown with that obtained by direct simulation as reference (Fig. 3b). The distribution is normalized to the peak in the reference. In this case, the separation distance d is 10 mm. The good agreement between the reconstructed results and the those obtained by the direct simulation is shown. In addition, Fig. 4 shows the results for a smaller separation distance of $d = 4$ mm. In this case, the peak value reconstructed at the center is slightly smaller than the that in the reference.

Using the APD in Figs. 3 and 4, the sAPD averaged over 4 cm^2 is also evaluated and the error is given as

$$\text{Err.} = 10\log_{10}\left(\frac{\text{sAPD}_{ref}}{\text{sAPD}_{rec}}\right), \quad (7)$$

where the denominator is the reconstructed sAPD and the

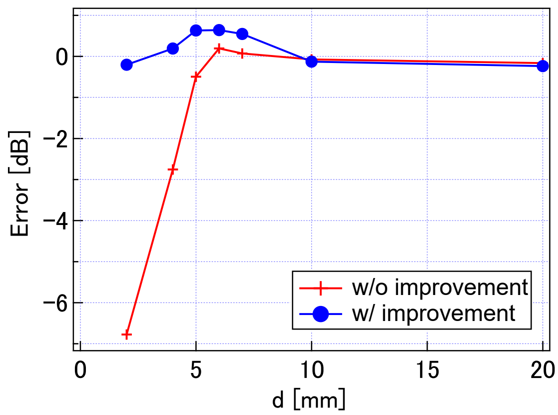

Figure 5. Error for various separation distances d. The red line shows the results without the improvement technique while the blue one with the improvement.

numerator is the reference obtained by the direct simulation. In the case of $d = 10$ mm, the error is -0.07 dB while the error is -2.8 dB in the case of $d = 4$ mm. In Fig. 5, error values for various separation distances are shown in the red line. The error is significantly smaller when the separation distance is larger. The error is well in the range ± 0.5 dB for $d \geq 5$ mm.

The reason for the accuracy degradation with decreasing separation distance is that S_{DUT} interrupts the propagation of information about the current on the phantom's surface, as discussed in [7]. For a smaller separation distance, a larger area is shadowed by S_{DUT}. Also, the information does not propagate through the phantom owing to absorption in the phantom. The loss of information in the shadowed area leads to the non-uniqueness and ill-conditioning of the matrix equation, and degrades the accuracy of the reconstructed results. More precisely, the non-uniqueness means that the solution space with a residual under a specific tolerance is expanded. Also, in such a case, the reconstructed results tend to show a lower APD because the iterative method with the initial solution of zero vector first converges to solutions with smaller norms in the expanded solution space.

A technique of reducing the effect of shadowing has also been proposed in [7]. In this technique, the iterative solver for the matrix equation is initialized with the solution of the lossless phantom ($\sigma = 0$). This technique is also tested in this example and the results in relation with the separation distance is also shown in Fig. 5 by a blue line. The accuracy is significantly improved especially in the smaller separation distances.

4 Conclusion

The reconstruction of the APD based on the surface equivalence theorem and PMCHWT formulation was studied. The method is based on the integral relationship between the electric field and the equivalent currents on the surface enclosing the DUT. The method gives the currents by solving the equation numerically with the iterative solver. In numerical experiments, the method showed accurate reconstruction results, especially when the separation distance between the DUT and the phantom was larger. Accuracy degradation as the DUT approached the phantom closer was also observed, which was due to shadowing on the phantom's surface. An accuracy improvement technique was also applied and found to be effective for small separation distances.

5 Acknowledgements

This work was supported by Ministry of Internal Affairs and Communications Grant Number JPMI10001.

References

[1] International Commission on Non-Ionizing Radiation Protection (ICNIRP), "Guidelines for limiting exposure to electromagnetic fields (100 kHz to 300 GHz)," *Health Physics*, vol. 118, pp. 483–524, may 2020.

[2] *IEEE Standard for Safety Levels with Respect to Human Exposure to Electric, Magnetic, and Electromagnetic Fields, 0 Hz to 300 GHz*. Standard IEEE C95.1-2019, 2019.

[3] S. Pfeifer, E. Carrasco, P. Crespo-Valero, E. Neufeld, S. Kuhn, T. Samaras, A. Christ, M. H. Capstick, and N. Kuster, "Total field reconstruction in the near field using pseudo-vector E-field measurements," *IEEE Transactions on Electromagnetic Compatibility*, vol. 61, no. 2, pp. 476–486, 2019.

[4] K. Sasaki, K. Li, J. Chakarothai, T. Iyama, T. Onishi, and S. Watanabe, "Error Analysis of a Near-Field Reconstruction Technique Based on Plane Wave Spectrum Expansion for Power Density Assessment above 6 GHz," *IEEE Access*, vol. 7, pp. 11591–11598, 2019.

[5] *Measurement procedure for the evaluation of power density related to human exposure to radio frequency fields from wireless communication devices operating between 6 GHz and 100 GHz*. IEC TR 63170, 2018.

[6] R. Mitharwal and F. P. Andriulli, "A regularised boundary element formulation for contactless SAR evaluations within homogeneous and inhomogeneous head phantoms," *Comptes Rendus Physique*, vol. 16, no. 9, pp. 776–788, 2015.

[7] S. Omi, T. Uno, T. Arima, and J. Wiart, "Reconstruction of Internal Field of Dielectric Objects for Noninvasive SAR Measurement Using Boundary Integral Equation," *IEEE Transactions on Electromagnetic Compatibility*, vol. 61, pp. 48–56, feb 2019.

[8] X. Q. Sheng, J. M. Jin, J. Song, W. C. Chew, and C. C. Lu, "Solution of combined-field integral equation using multilevel fast multipole algorithm for scattering by homogeneous bodies," *IEEE Transactions on Antennas and Propagation*, vol. 46, no. 11, pp. 1718–1726, 1998.

[9] J.-M. Jin, *Theory and Computation of Electromagnetic Fields*. Hoboken, NJ, USA: John Wiley & Sons, Inc., nov 2010.

[10] W. C. Gibson, *The Method of Moments in Electromagnetics*. Chapman & Hall/CRC, 2008.

[11] C. C. Paige and M. A. Saunders, "LSQR: an algorithm for sparse linear equations and sparse least squares," *ACM Transactions on Mathematical Software*, vol. 8, no. 1, pp. 43–71, 1982.

[12] Altair FEKO 2020. Accessed: Jan. 18, 2021. [Online]. Available: `https://altairhyperworks.com/product/FEKO`.